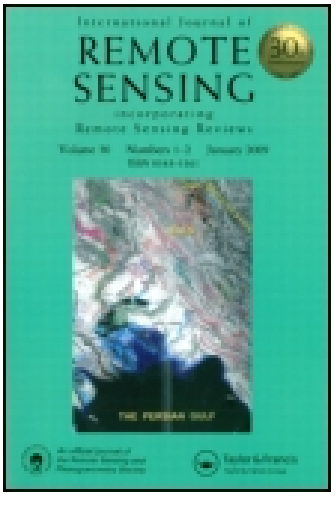

International Journal of Remote Sensing
Publication details, including instructions for authors and subscription information:
http://www.tandfonline.com/loi/tres20

Uncertainty analysis of five satellite-based precipitation products and evaluation of three optimally merged multi-algorithm products over the Tibetan Plateau

Yan Shen[a], Anyuan Xiong[a], Yang Hong[bcd], Jingjing Yu[a], Yang Pan[a], Zhuoqi Chen[e] & Manabendra Saharia[bc]

[a] National Meteorological Information Centre, Beijing 100081, China

[b] School of Civil Engineering and Environmental Science, University of Oklahoma, Norman, OK 73072, USA

[c] Advanced Radar Research Center, National Weather Center, Norman, OK 73072, USA

[d] Department of Hydraulic Engineering, Tsinghua University, Beijing, China

[e] College of Global Change and Earth System Science, Beijing Normal University, Beijing 100875, China

Published online: 08 Oct 2014.

To cite this article: Yan Shen, Anyuan Xiong, Yang Hong, Jingjing Yu, Yang Pan, Zhuoqi Chen & Manabendra Saharia (2014) Uncertainty analysis of five satellite-based precipitation products and evaluation of three optimally merged multi-algorithm products over the Tibetan Plateau, International Journal of Remote Sensing, 35:19, 6843-6858, DOI: 10.1080/01431161.2014.960612

To link to this article: http://dx.doi.org/10.1080/01431161.2014.960612

International Journal of Remote Sensing, 2014
Vol. 35, No. 19, 6843–6858, http://dx.doi.org/10.1080/01431161.2014.960612

Uncertainty analysis of five satellite-based precipitation products and evaluation of three optimally merged multi-algorithm products over the Tibetan Plateau

Yan Shen[a], Anyuan Xiong[a], Yang Hong[b,c,d]*, Jingjing Yu[a], Yang Pan[a], Zhuoqi Chen[e], and Manabendra Saharia[b,c]

[a]*National Meteorological Information Centre, Beijing 100081, China;* [b]*School of Civil Engineering and Environmental Science, University of Oklahoma, Norman, OK 73072, USA;* [c]*Advanced Radar Research Center, National Weather Center, Norman, OK 73072, USA;* [d]*Department of Hydraulic Engineering, Tsinghua University, Beijing, China;* [e]*College of Global Change and Earth System Science, Beijing Normal University, Beijing 100875, China*

(*Received 9 September 2013; accepted 4 August 2014*)

This study is the first comprehensive examination of uncertainty with respect to region, season, rain rate, topography, and snow cover of five mainstream satellite-based precipitation products over the Tibetan Plateau (TP) for the period 2005–2007. It further investigates three merging approaches in order to provide the best possible products for climate and hydrology research studies. Spatial distribution of uncertainty varies from higher uncertainty in the eastern and southern TP and relatively smaller uncertainty in the western and northern TP. The uncertainty is highly seasonal, temporally varying with a decreasing trend from January to April and then remaining relatively low and increasing after October, with an obvious winter peak and summer valley. Overall, the uncertainty also shows an exponentially decreasing trend with higher rainfall rates. The effect of topography on the uncertainty tends to rapidly increase when elevation exceeds 4000 m, while the impact slowly decreases in areas lower than that topography. The influence of the elevation on the uncertainty is significant for all seasons except for the summer. Further cross-investigation found that the uncertainty trend is highly correlated with the MODIS-derived snow cover fraction (SCF) time series over the TP (e.g. correlation coefficient ≥0.75). Finally, to reduce the still relatively large and complex uncertainty over the TP, three data merging methods are examined to provide the best possible satellite precipitation data by optimally combining the five products. The three merging methods – arithmetic mean, inverse-error-square weight, and one-outlier-removed arithmetic mean – show insignificant yet subtle differences. The Bias and RMSE of the three merging methods is dependent on the seasons, but the one-outlier-removed method is more robust and its result outperforms the five individual products in all the seasons except for the winter. The correlation coefficient of the three merging methods is consistently higher than any of five individual satellite estimates, indicating the superiority of the method. This optimally merging multi-algorithm method is a cost-effective way to provide satellite precipitation data of better quality with less uncertainty over the TP in the present era prior to the Global Precipitaton Measurement Mission.

1. Introduction

The Tibetan Plateau (TP), known as the Earth's third pole, is the world's highest plateau, averaging over 4000 m above sea level. It has a great influence on regional and even global

*Corresponding author. Email: yanghong@ou.edu

climate change and disastrous weather arising from anomalous thermal and dynamic processes over it (Luo and Yanai 1984). High-quality precipitation observation is important for understanding the thermal and dynamic processes over the TP. Precipitation at each grid box is also required for driving land surface and hydrological models. But, because of its complex terrain and harsh natural environment, very few gauges and meteorological radars are installed in the southeast of the TP, and there are no gauges or radar in the vast areas of the southern and western TP. Fortunately, with the development of remote-sensing technology, several satellite-based precipitation retrieval algorithms have been developed, and their related precipitation products are available now (Joyce et al. 2004; Hong, Hsu, and Sorooshian 2004; Hsu et al. 1997, 1999; Sorooshian et al. 2000; Turk et al. 2003; Huffman and Adler 2007; Hsu et al. 2009). However, satellite-based retrieval is an indirect way to obtain precipitation estimates, and different retrieval algorithms tend to have their own merits and demerits, quantified by uncertainty measures as a function of space, time, and rainfall intensity (Ebert, Janowiak, and Kidd 2007; Tian et al. 2007, 2009; Shen, Xiong, et al. 2010; Yong et al. 2012; Chen et al. 2013). Tian and Peters-Lidard (2010) proposed to estimate global precipitation uncertainties as a variable of the rain rate at given locations among many other studies (Adler et al. 2001; Smith et al. 2006; Adler et al. 2009). To the best of our knowledge, uncertainty over the TP has not yet been fully studied with all available mesoscale satellite precipitation products. In this study, five mainstream satellite-based precipitation products are comprehensively examined for the first time over the TP for the period 2005–2007. The uncertainty is examined and quantified with factors considering space, season, and rain rate, as Tian and Peters-Lidard (2010) did. On the other hand, the influence of snow cover change and topographic features on the uncertainty is also investigated owing to the high elevation of the TP.

Building an ensemble average forecast field by the results from different methods, different models, or the different forecast members of the same model has been widely studied and applied in meteorology (Sanders 1963) and hydrology (McLeod et al. 1987). The advantage of the ensemble average is that it is able to effectively synthesize forecast information of multiple members in order to obtain higher forecast skill than a single member. However, Li (2011) reported that the ensemble prediction does not always provide a more accurate forecast field than a single forecast. In this study, ensemble prediction is employed to provide the best satellite precipitation data for numerous research studies and applications over the sparsely gauged TP. Here, three ensemble methods – arithmetic mean, inverse-error-square weight, and one-outlier-removed arithmetic mean – are introduced, and results are compared to the five individual satellite data sources both at seasonal and at annual time scales.

The following sections will first describe the study area, data, and method, followed by uncertainty analysis, data ensemble investigation, and conclusions.

2. Study area, data, and method

The study area is 25–40° N and 75–105° E, confining the TP region over the 3-year period of 2005–2007. A dense national gauge network of ~330 gauges has been established within the research region as shown in Figure 1. The average distance between gauges is 78.9 km. If the latitude line of 100° E is used to divide the research area into two sub-regions, east and west, the gauge number (average gauge-to-gauge distance) for western and eastern parts is ~110 (133.1 km) and 220 (55.5 km), respectively, indicating a much denser gauge network in the east and a relatively sparse one in the west. The gauge observations have gone through three levels of quality control and are then

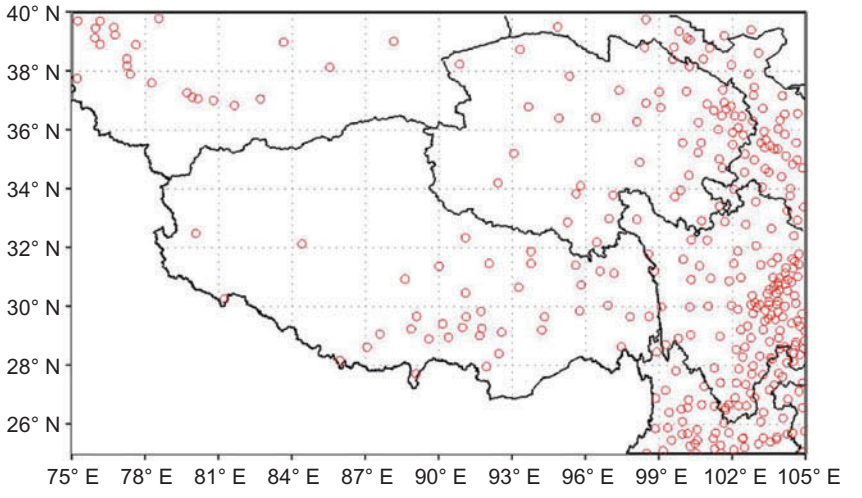

Figure 1. Gauge distribution over the research area (one red circle represents one gauge, black line at the position of 100° E is used to divide the research area into two parts, east and west).

accumulated into daily gauge-site precipitation data. These quality-controlled point data are used to generate the gauge-based precipitation analysis (GPA) at a 0.25° grid box (Shen, Feng, et al. 2010) using the optimal interpolation method first proposed by Xie et al. (2007), with additional topographic corrections. In this process, topographic effect is adjusted by following the method used in PRISM (Parameter-elevation Regressions on Independent Slopes Model) data analysis (Daly, Neilsen, and Phillips 1994). Figure 2 (*a*)–(*e*) shows the spatial distribution of the 3-year mean annual and seasonal precipitation from GPA. Mean precipitation distribution over the TP is characterized by an east-to-west decreasing trend. A large amount of precipitation is observed over the eastern and south-eastern TP, and the temporal distribution has seasonal dependence with a high (low) amount in warm (cold) seasons.

Five level-3 satellite-based precipitation estimates by blending passive microwave (PMW) and infrared (IR) sensors are used in this article. They are: (1) global precipitation fields generated by the National Oceanic and Atmospheric Administration (NOAA) Climate Prediction Center (CPC) morphing technique (CMORPH) (Joyce et al. 2004); (2) Precipitation Estimation From Remotely Sensed Information Using Artificial Neural Network (PERSIANN) (Hsu et al. 1997, 1999); (3) the Naval Research Laboratory (NRL) blended satellite precipitation estimates (Turk et al. 2003); (4) Tropical Rainfall Measuring Mission (TRMM) precipitation products 3B42 version 7; and (5) its real-time version 3B42RT (Huffman and Adler 2007). The main differences in the five products arise from two factors: one is the input satellite sources and the other is the IR-PMW merging algorithms. The related information about the five satellite products is included in Table 1.

The method used in this article is the three merging approaches – arithmetic mean, inverse-error-square weight, and one-outlier-removed arithmetic mean – as follows:

$$R_1 = \frac{1}{n}\sum_{k=1}^{n} S_k, \tag{1}$$

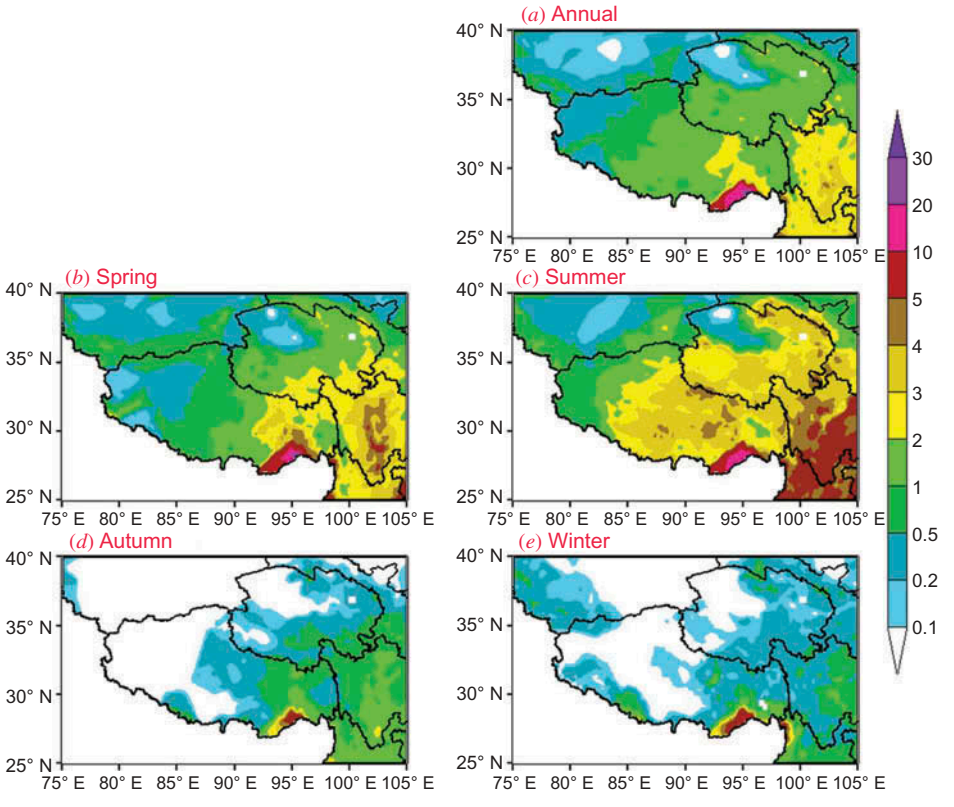

Figure 2. (*a–e*) The 2005–2007 mean annual and seasonal precipitation distribution from GPA over the TP (unit: mm day^{-1}).

Table 1. Information of five satellite-based precipitation products used in this research.

Product name	Provider	Input data	Retrieval algorithm
Precipitation Estimation from Remotely Sensed Information using Artificial Neural Networks (PERSIANN)	UC Irvine (Hsu K.-L.)	IR : GOES-IR; PMW: TRMM 2A12	Adaptive artificial neural network
Naval Research Laboratory blended algorithm (NRL)	NRL (Turk J.)	IR : Geo-IR; PMW: SSM/I, TRMM, AMSU, AMSR	Histogram matching method
TRMM multi-satellite precipitation analysis (3B42RT for real time or 3B42 Version 7)	GSFC (Huffman G.)	IR : Geo-IR PMW: TMI, SSMI, SSMIS, AMSR-E, AMSU-B, MHS	3B42RT: histogram matching method 3B42: GPCC monthly gauge observations to correct the bias of 3B42RT
CPC morphing technique (CMORPH)	NOAA CPC (Joyce B.)	IR : Geo-IR; PMW: SSMI, AMSU-B, TMI, AMSR-E	CPC morphing technique: first, the vector of the cloud motion is calculated by the IR data, then the rainfall from the PMW exclusively is transported based on the motion vector

$$R_2 = \frac{1}{n}\sum_{k=1}^{n} W_k \times S_{k,} W_K = \frac{1}{\sigma_K^2}, \tag{2}$$

$$R_3 = \frac{1}{n-1}\sum_{k=1}^{n-1} S_k, \tag{3}$$

where, R_1, R_2, and R_3 are the precipitation obtained from the arithmetic mean, inverse-error-square weight, and one-outlier-removed arithmetic mean, respectively. S_k is a satellite-based precipitation product, n is the number of satellite products examined, and $n = 5$ in this article. W_K is the weighting factor that is a function of the inverse proportion to the error square (σ_K^2) for each satellite product. All values are calculated both at the spatial and at the temporal scales. The spatial scale is a 0.25° grid box with at least one gauge available over the TP and the temporal scale is daily for the period 2005–2007.

Several common statistical indices are used to quantitatively evaluate individual algorithms and the merged ensemble estimates with GPA including Bias, relative bias (R_{Bias}), root-mean-square error (RMSE), and correlation coefficient (CC). Additionally, a set of contingency table statistics is used in this study. They are probability of detection (POD), false-alarm ratio (FAR), critical success index (CSI), and equitable threat score (ETS) (Ebert, Janowiak, and Kidd 2007). All analyses in this article are done just for grid boxes with at least one gauge available to ensure statistical significance and less interpolated error.

3. Uncertainty analysis

3.1. *Spatial distribution*

GPA is conventionally used to quantify the uncertainty of satellite products, but its limited distribution makes it less representative. Satellite products have full spatial coverage, and so they can be used to examine the uncertainty of the satellite-based precipitation estimates over the whole region. The standard deviation of five satellite products is calculated first and uncertainty is defined as the ratio of standard deviation to mean daily precipitation from five satellite products. Because precipitation with rain rate less than 0.5 mm day^{-1} accounts for almost 80% of the total amount of rainfall, especially in winter, which will lead to unreliable uncertainty, standard deviation is used when plotting the spatial distribution of uncertainty. The spatial distribution of annual and seasonal uncertainties over the TP for 2005–2007 is shown in Figures 3(*b*)–(*f*). The elevation of the research domain is also in Figure 3(*a*). The spatial uncertainty is dependent on seasons. The maximum uncertainty is more than 5.0 mm day^{-1} and is always distributed in the southeastern TP where the elevation changes sharply from 3000 m to more than 5000 m. In the western and northern TP, uncertainty is relatively small, with values less than 3.0 mm day^{-1}. It indicates that precipitation estimates from different satellite retrieval algorithms generally have better agreement in the western and northern TP than in the southeastern TP.

3.2. *SCF-dependent seasonal uncertainty*

Figure 4 shows the seasonality time series of mean relative uncertainty of satellite precipitation estimates for 2005–2007. The uncertainty decreases from January to April,

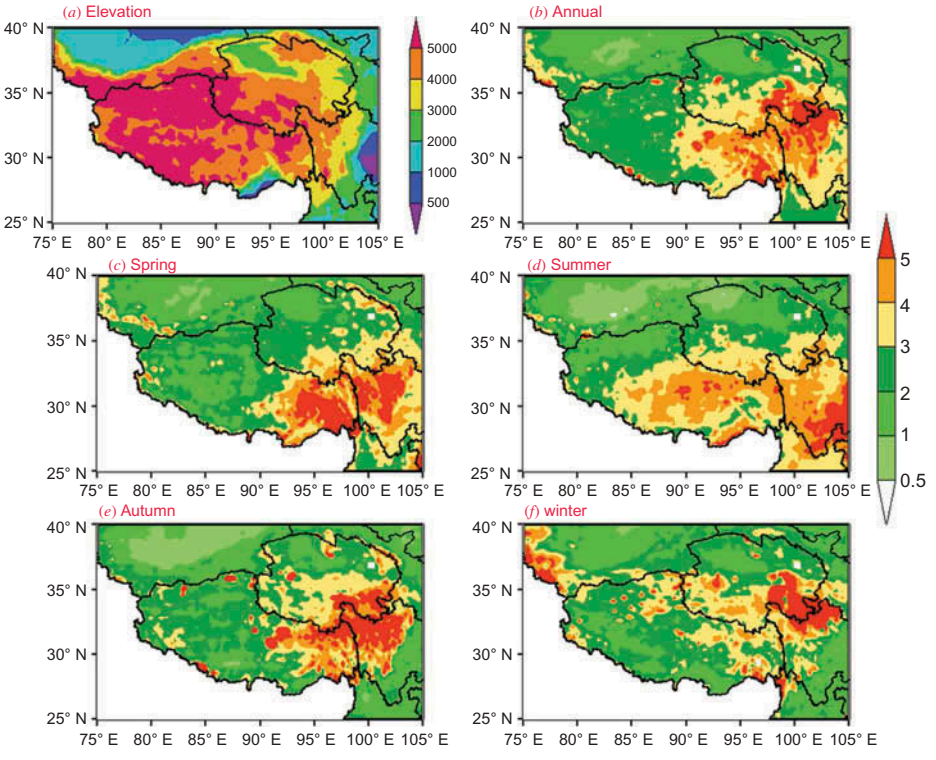

Figure 3. (*a–f*) Spatial distribution of uncertainty (unit: mm day^{-1}) for 2005–2007 and the elevation (unit: m) over the TP.

then remains relatively low, and increases after October. The uncertainty of satellite precipitation estimates shows a fluctuation from 136.02% to 319.63%, with a mean value of 211.99%. Given the current limitation of satellite precipitation sensors in detection of solid precipitation, we suspect that the uncertainty is probably associated with snowfall seasonality over the TP. Thus, we further investigated the uncertainty connection with snow cover fraction (SCF) derived from MODIS daily snow data (MODIS user guide 2003) in Figure 4, where SCF is defined as the ratio between snow-covered grid boxes and total grid boxes over the research domain. As shown in Figure 4, SCF temporally fluctuates between 5.27% and 32.15%, with a mean value of 14.40%. As anticipated, the time series of SCF shows a very good agreement with the seasonal uncertainty of satellite precipitation given their relatively high correlation coefficient (between two time series is 0.75). The warm season from April to September is a period with relatively low uncertainty and SCF with a mean of 179.23% and 10.04%, respectively. However, the related value for the cold season from October to the following March is 244.93% and 18.67%, respectively. The higher/lower uncertainty is related to the relatively high/low SCF. This clearly indicates that the current spaceborne quantitative precipitation estimation (QPE) is incapable of adequately resolving winter precipitation. Meanwhile, the recently launched Global Precipitation Measurement Mission, with dual-frequency precipitation radar and multi-frequency passive microwave channels, holds promising potential in this regard.

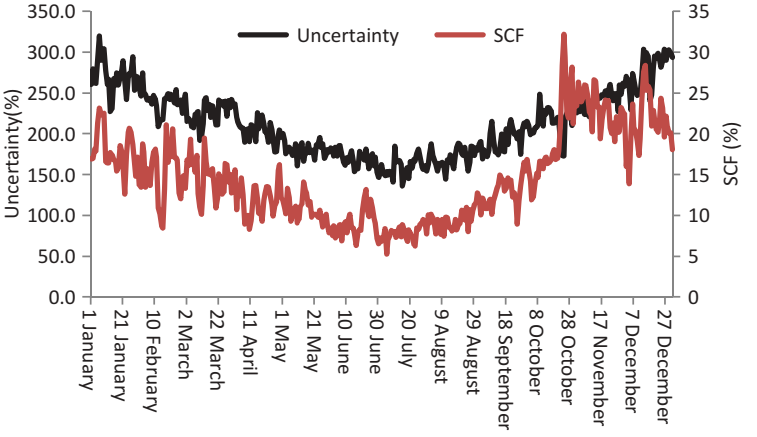

Figure 4. Seasonality of mean relative uncertainty (unit: %) of satellite precipitation estimates and mean of SCF (unit: %) from MODIS data averaged for the 2005–2007 period over the TP.

3.3. *Rain rate-dependent uncertainty*

Influence of rainfall rate on the uncertainty was previously investigated by Tian and Peters-Lidard (2010) among others in different parts of the world except in the TP. In this study, different rain rate categories are classified based on the mean data of five satellite products. According to the rain rate, the uncertainty is calculated at each grid box for four seasons and annual mean (Figure 5). It shows that the uncertainty decreases with the rain rate. In summer, the uncertainty is 160% with the rain rate category in 0.0–0.5 mm day^{-1} while the uncertainty is reduced to 40% at the rain rate ≥ 20.0 mm day^{-1}. Moreover, the uncertainty is seasonally dependent with the smallest in summer and the largest in winter. For example, when the rain rate has fallen to 5.0–10.0 mm day^{-1}, uncertainty is 73.3% and 110.2% for summer and winter, respectively.

3.4. *Topography-dependent uncertainty*

Topography has a great and complex effect on precipitation. Four elevation categories are classified as (1) elevation < 2000 m; (2) 2000 m ≤ elevation < 3000 m; (3)

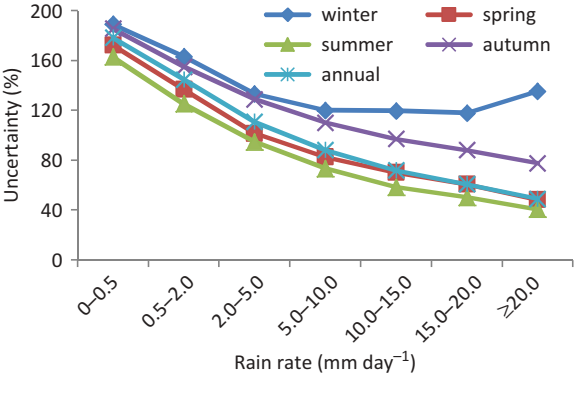

Figure 5. The relationship between uncertainties and rain rate for annual mean and four seasons over the TP for 2005–2007.

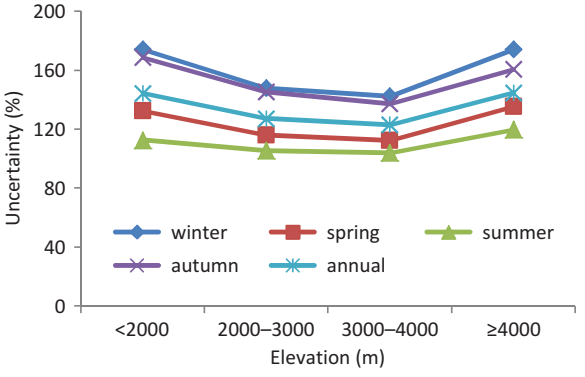

Figure 6. The relationship between uncertainty (unit: %) and elevation (unit: m) for annual mean and four seasons over the TP for 2005–2007.

3000 m ≤ elevation < 4000 m; and (4) elevation ≥ 4000 m. The uncertainty is calculated at each grid box. Then the seasonal and annual uncertainty is averaged according to the elevation categories (Figure 6). In general, the effect of topography on the uncertainty tends to gradually decrease when the elevation is less than 4000 m, and uncertainty increases fast with an elevation larger than 4000 m. The trend is relatively small in summer but large in winter. Moreover, the seasonal and annual uncertainty of satellite-based precipitation products is investigated as a function of the different elevation points. A region encompassed by 28°–35° N and 92°–104° E is selected because of its dramatic change of elevation and relatively dense network. Based on the gauge analysis over the grid box, with at least one gauge available, the meridional distribution from 92° E to 104° E of seasonal and annual uncertainty for five satellite-based precipitation products is shown in Figure 7 together with the average elevation taking 28°–35° N as the cross-section. The mean elevation is decreased from 5119 m to 988 m,

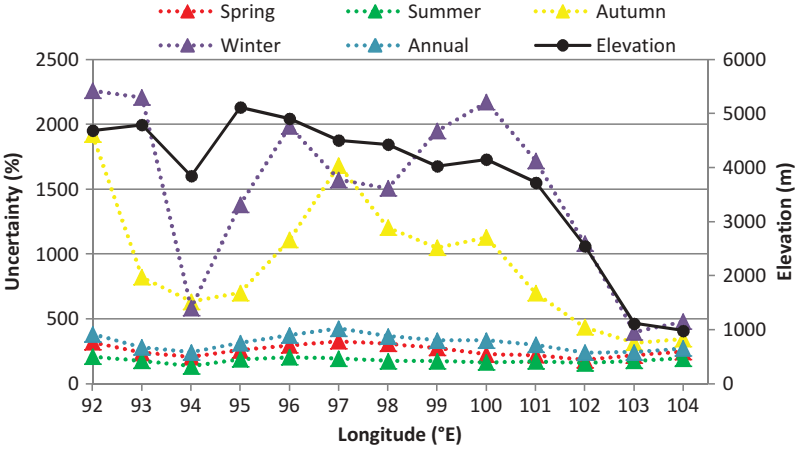

Figure 7. The meridional distribution from 92° E to 104° E of seasonal and annual uncertainty for five satellite-based precipitation products together with the average elevation taking 28° N–35° N as the cross-section for 2005–2007.

and the range of elevation is more than 4000 m when the longitude is changed from 92° E to 104° E. The uncertainty of five satellite-based precipitation products is dependent on the elevation points. Taking 94° E and 95° E as the dividing points, the elevation is decreased at first, then increases, and then decreases gradually. The same feature is exhibited for the seasonal and annual uncertainty of satellite products, especially for the winter and autumn seasons. The correlation coefficient between uncertainty for winter and autumn seasons and the elevation reaches at 0.77 and 0.67, respectively. It is 0.51 for the spring season. The influence of the elevation on the uncertainty is minimum in summer and the correlation coefficient is only 0.17. The correlation coefficient between the annual uncertainty and the elevation is still 0.63, indicating the great effect of the elevation on the annual uncertainty. In addition to the relatively small effect of the elevation on the uncertainty in summer, the effect of the elevation on the other seasonal uncertainty is significant, particularly in the winter and autumn.

4. Uncertainty analysis of the merged multi-algorithm data ensembles

Owing to relatively large uncertainty and limited observations over the TP, it is beneficial to further improve the precipitation quality by captalizing on the strengths of all available satellite precipitation products. Thus, we evaluate the performance of three ensemble methods for generating the best possible merged satellite precipitation data. They are arithmetic mean, inverse-error-square weight, and one-outlier-removed arithmetic mean, as shown in Section 2.

4.1. Statistical analysis

Tables 2 and 3 summarize the comparison statistics for the five satellite products and the three ensembles at daily and 0.25° resolution over the TP for summer and winter of 2005–2007, respectively. Bias of each individual satellite precipitation estimation ranges from −0.736 mm day^{-1} to 1.830 mm day^{-1} and RMSE ranges from 4.492 mm day^{-1} for CMORPH to 6.793 mm day^{-1} for PERSIANN. However, Bias (RMSE) between the ensembles and GPA are much reduced from −0.475 to 0.208 mm day^{-1} (4.184 mm day^{-1} to 4.247 mm day^{-1}), which is better than that between any of five individual satellite estimates and gauge observations. The ensemble data produced by the inverse-error-square weight has the best performance with Bias (relative bias) of −0.056 mm day^{-1} (−1.9%) among all three ensemble products, while the ensemble data produced by the

Table 2. Evaluation results of GPA *versus* five satellite estimates and three satellite ensembles over the TP for the summer period of 2005–2007.

	Bias	R_{Bias}	RMSE	R_{RMSE}	CC
CMORPH	−0.736	−0.253	4.492	1.546	0.568
PERSIANN	1.830	0.630	6.793	2.338	0.502
NRL	0.713	0.246	6.188	2.130	0.478
TRMM/3B42	−0.252	−0.087	5.337	1.837	0.507
3B42RT	0.324	0.112	5.391	1.855	0.506
Arithmetic mean	0.208	0.072	4.247	1.462	**0.634**
Inverse-error-square	**−0.056**	**0.019**	4.228	1.455	0.633
One-outlier-removed	−0.475	−0.164	**4.184**	**1.440**	0.625

Note: Bold values are the best result obtained for a particular product and for each statistical parameter.

Table 3. Evaluation results of GPA *versus* five satellite estimates and three satellite ensembles over the TP for the winter period of 2005–2007.

	Bias	R_{Bias}	RMSE	R_{RMSE}	CC
CMORPH	0.035	0.147	1.840	7.625	0.051
PERSIANN	1.686	6.990	4.228	17.527	0.153
NRL	1.684	6.981	5.721	23.713	0.056
TRMM/3B42	**−0.003**	**−0.014**	**1.728**	**7.161**	**0.265**
3B42RT	0.873	3.618	3.414	14.152	0.163
Arithmetic mean	0.767	3.179	2.151	8.916	0.184
Inverse-error-square	0.419	1.738	1.930	7.999	0.196
One-outlier-removed	0.185	0.766	1.733	7.185	0.197

Note: Bold values are the best result obtained for a particular product and for each statistical parameter.

one-outlier-removed method provides the smallest RMSE (4.184 mm day^{-1}). Correlation coefficients from the three ensembles ranging from 0.625 to 0.634 are much larger than the best value from the individual satellite product (0.568 in CMORPH). These results suggest that quality of assembling different satellite products is further improved by capitalizing on each individual product with proper ensemble methods, resulting in a relatively lower bias and RMSE and a higher correlation. For the winter period, Bias from the one-outlier-removed method presents the smallest value of 0.185 mm day^{-1} in the three merging algorithms, but it is still larger than the best value of −0.003 mm day^{-1} obtained from the TRMM 3B42. The similar characteristic is for the correlation coefficient changing from 0.184 to 0.197 from the ensembles, but it is lower than the best value from TRMM 3B42 (0.265). The RMSE obtained from the one-outlier-removed method is 1.733 mm day^{-1}, which is at the same level as the best value from TRMM 3B42 (1.728 mm day^{-1}). The difference of three merging algorithms is increased, and the result from the one-outlier-removed method is better than other two methods, but it is still worse than that from TRMM 3B42. For each single satellite precipitation estimate, the bias shows a relatively large range from only −0.003 mm day^{-1} for TRMM 3B42 to 1.686 mm day^{-1} for PERSIANN, with a difference of 1.689 mm day^{-1}. The same characteristic is for the RMSE changing from 1.728 mm day^{-1} for TRMM 3B42 to 5.721 mm day^{-1} for NRL, with a difference of 3.993 mm day^{-1}. Bias and RMSE among five satellite products is a large varying amplitude and TRMM 3B42 is significantly better than other single satellite products in winter, which lead to the failure of the ensemble data. This result has been proved in the field of the ensemble prediction for numerical weather models (Li 2011; Yoo and Kang 2005; Jeong and Kim 2009; Winter and Nychka 2010) and is first confirmed and extended in the field of satellite precipitation estimates.

When the rainfall threshold is selected as 0.1 mm day^{-1}, values of ETS, CSI, POD, and FAR for five satellite precipitation estimates and three merged ensembles over the TP for the summer and winter periods during 2005–2007 are shown in Tables 4 and 5, respectively. These indices are calculated against GPA grids that contain at least one gauge. In summer, ETS, CSI, and FAR for five satellite precipitation estimates are very close, except that POD for five satellite estimates has a large amplitude from 0.73 for TRMM/3B42 to 0.82 for PERSIANN. CSI and POD for the ensembles are increased compared with those for five satellite estimates. The highest CSI in five satellite estimates is 0.67, while that for ensembles is 0.69. It indicates that the ensembles can detect more rainfall events than individual satellite estimates. FAR for the ensembles in the rainfall

Table 4. Values of ETS, CSI, POD, and FAR for five satellite estimates and three satellite ensembles over the TP for the summer period of 2005–2007.

	ETS	CSI	POD	FAR
CMORPH	0.24	0.64	0.79	0.23
PERSIANN	**0.28**	0.67	0.82	0.22
NRL	0.24	0.65	0.81	0.24
TRMM/3B42	0.24	0.61	0.73	**0.21**
3B42RT	0.21	0.61	0.75	0.24
Arithmetic mean	0.24	**0.69**	**0.93**	0.27
Inverse-error-square	0.27	**0.69**	0.89	0.25
One-outlier-removed	**0.28**	**0.69**	0.87	0.23

Notes: The rainfall threshold is 0.1 mm day^{-1}. Bold values are the best result obtained for a particular product and for each statistical parameter.

Table 5. Values of ETS, CSI, POD, and FAR for five satellite estimates and three satellite ensembles over the TP for the winter period of 2005–2007.

	ETS	CSI	POD	FAR
CMORPH	0.03	0.12	0.33	0.84
PERSIANN	0.07	0.18	0.85	0.81
NRL	0.05	0.16	0.62	0.83
TRMM/3B42	**0.14**	**0.21**	0.39	**0.69**
3B42RT	0.09	0.19	0.58	0.78
Arithmetic mean	0.05	0.17	**0.94**	0.83
Inverse-error-square	0.09	0.20	0.82	0.79
One-outlier-removed	0.10	0.20	0.74	0.78

Notes: The rainfall threshold is 0.1 mm day^{-1}. Bold values are the best result obtained for a particular product and for each statistical parameter.

threshold of 0.1 mm day^{-1} is a little enhanced compared to that from individual products; however, further investigation shows that when a higher rainfall threshold such as 5.0 mm day^{-1} is selected, FAR for the ensembles will be smaller. The merged ensemble is an effective way to correctly detect more rainfall events and reduce missed and false events. In winter, however, ETS, CSI, POD, and FAR from the five satellite products present a relatively large changing amplitude. ETS (TS) changes from 0.03 (0.12) for CMORPH to 0.14 (0.21) for TRMM 3B42 while POD (FAR) varies from 0.33 (0.84) for CMORPH to 0.85 (0.69) for PERSIANN (TRMM 3B42). The best value for each of the four parameters is not consistently obtained from the three merging algorithms, especially for the ETS and FAR. ETS (FAR) changes from 0.05 (0.78) to 0.1 (0.83) from the three merging algorithms, and it is still lower (higher) than the best value of 0.14 (0.69) from the TRMM 3B42. CSI changing from 0.17 to 0.2 by the three merging algorithms is almost at the same level as the best value in five individual satellite products (0.21 from TRMM 3B42). The improvement of POD is obvious for the highest value of 0.85 from PERSIANN to 0.94 from the ensemble of the arithmetic mean.

4.2. Spatial distribution

The spatial distribution of the annual mean uncertainty for the ensemble is shown in Figure 8 together with the five satellite-based precipitation products in order to examine

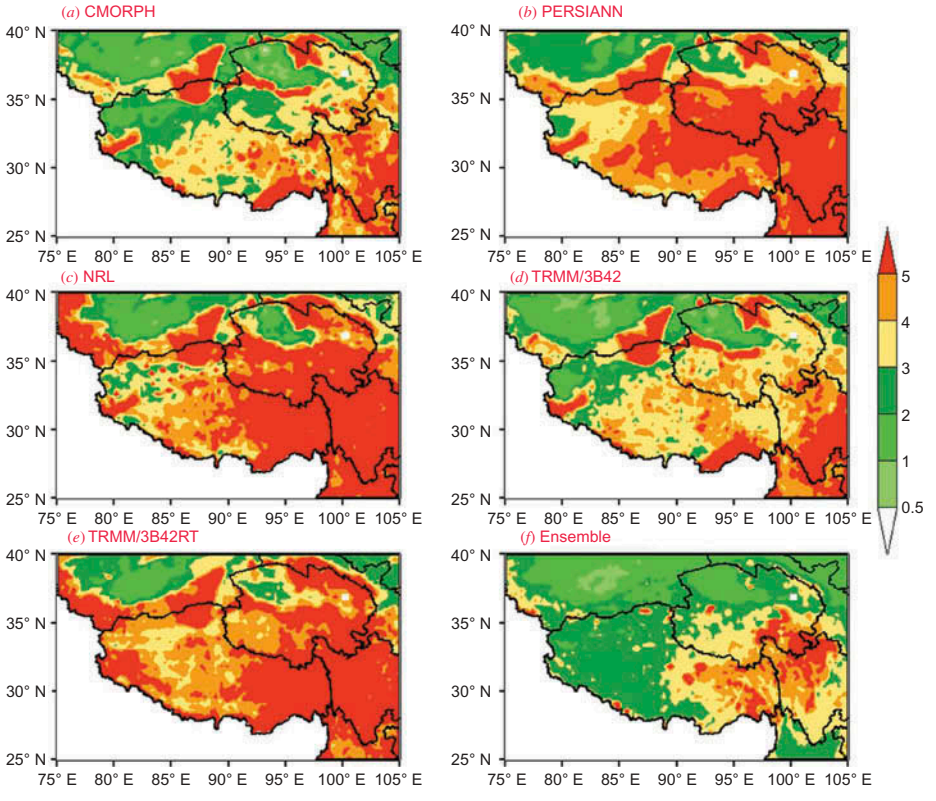

Figure 8. (*a–f*) The 2005–2007 annual mean spatial distribution of uncertainty for five satellite products and the ensemble from the inverse-error-square weight method over the TP.

which of the satellite products contribute more to the uncertainty. Compared with the uncertainty of PERSIANN, NRL, and TRMM 3B42RT, uncertainty of TRMM 3B42 and CMORPH is relatively small, but it is still larger than that of the ensemble over the entire research. There is no existing gauge in the western part of the TP where uncertainty from each of five satellite products is more than 3 mm day^{-1}. The ensemble data show a very small uncertainty with a value of less than 3 mm day^{-1} after merging the five products. It indicates that the ensemble has the smallest uncertainty among the five products. The same feature is depicted at the four seasonal time scales, which are omitted to avoid redundancy. To further investigate which of the satellite products contributes more to the uncertainty in a qualitative sense, the number of each satellite product being taken as the outlier is calculated for 2005–2007, as shown in Table 6. The outlier satellite product has the largest deviation from the arithmetic mean at each grid box and time. Among the five satellite products, only TRMM 3B42 uses the gauge data to correct the bias and TRMM 3B42 has the minimum (455,129) number being taken as the outlier in the research domain and period. The procedure of cloud classification and snow screening is not considered in the PERSIANN algorithm, which leads to the maximum number (2,326,270) being taken as the outlier. The result of outlier number for each satellite product can demonstrate that the PERSIANN product contributes the most to the uncertainty qualitatively, followed by TRMM 3B42RT (1,305,663), NRL (1,295,385), CMORPH (489,789), and TRMM 3B42 (455,129).

Table 6. Number of each satellite products being taken as the outlier over the TP for 2005–2007.

	CMORPH	PERSIANN	NRL	3B42	3B42RT
Number	489,789	2,326,270	1,295,385	455,129	1,305,663

Table 7. Evaluation results of GPA *versus* 3 satellite ensembles and combining CMORPH with TRMM 3B42 (CMORPH+3B42) over the TP at the seasonal and annual time scales for 2005–2007.

	Arithmetic mean			Inverse-error-square			One-outlier-removed			CMORPH+3B42		
	Bias	RMSE	CC	Bias	RMSE	CC	Bias	RMSE	CC	Bias	RMSE	CC
Spring	0.892	3.671	0.511	0.567	3.589	0.520	**0.110**	3.408	**0.533**	−0.301	**3.374**	0.518
Summer	0.208	4.247	**0.634**	**−0.056**	4.228	0.633	−0.475	**4.184**	0.625	−0.494	4.338	0.601
Autumn	1.059	2.579	0.362	0.738	2.256	0.398	0.448	1.963	**0.433**	**0.263**	**1.943**	0.362
Winter	0.767	2.151	0.184	0.419	1.930	0.196	0.185	1.733	0.197	**0.016**	**1.652**	**0.226**
Annual	0.712	3.351	0.573	0.400	3.231	0.589	**0.044**	**3.096**	**0.597**	−0.148	3.127	0.583

Notes: The rainfall threshold is 0.1 mm day^{-1}. Bold values are the best result obtained for a particular season and for each statistical parameter.

CMORPH and TRMM 3B42 products show smaller RMSE and lower number being taken as the outlier over the spatial scale, so another question arises whether combining CMORPH with TRMM 3B42 can provide better estimates than the three ensembles used in the article. Table 7 shows the evaluation results of three ensembles and a combination of CMORPH and TRMM 3B42 *versus* the GPA over the grid box, with at least one gauge available at the seasonal and annual time scales. Bold values are the best results obtained for a particular season and each statistical parameter. Although the evaluation results are dependent on the merging methods for a particular season, the result from the one-outlier-removed arithmetic mean is more stable and reliable. For example, the statistics index of Bias, RMSE, and CC from the one-outlier-removed arithmetic mean is consistently the best among the four methods at the annual time scale. Bias is 0.044 mm day^{-1}, RMSE is 3.096 mm day^{-1}, and CC is 0.597. In summer, CC from the arithmetic mean (0.634) and Bias from the inverse-error-square weight (−0.056 mm day^{-1}) are the best but RMSE from the one-outlier-removed arithmetic mean (4.184 mm day^{-1}) is the smallest. However, the result from combining CMORPH with TRMM 3B42 has the advantage in the cold seasons of autumn and winter, which shows the smallest Bias (0.016 mm day^{-1}), RMSE (1.652 mm day^{-1}), and highest correlation coefficient (0.226) among the four ensemble data, but it is still worse than the result from TRMM 3B42.

5. Conclusions

In this study, uncertainty of five state-of-the-art satellite-based precipitation estimates has been comprehensively evaluated for the first time with respect to region, season, elevation, rain intensity, snow cover, and topography over the TP spanning the period of 2005–2007 due to the satellite product availability. Also, three merging methods are further investigated in order to provide one best possible spaceborne precipitation product for climate and hydrology research. Major conclusions are summarized below.

(1) The uncertainty map over the TP is produced for five satellite precipitation estimates, and shows strong regional and seasonal dependencies. Larger uncertainty is distributed in the east–southern TP, and relatively small uncertainty is in the western and northern TP. Uncertainty has high seasonality, temporally changing with a decreasing trend from January to April, then remaining at a relatively low value, and increasing after October, with an obvious winter peak and summer valley.

(2) Overall, the uncertainty also shows an exponentially decreasing trend with higher rainfall rates. Additionally, the effect of topography on the uncertainty tends to rapidly increase when the elevation higher than 4000 m, while the impact slowly decreases in areas lower than that topography. The effect of elevation on the uncertainty is significant for all seasons except the summer.

(3) Further cross-investigations indicate that the uncertainty seasonality has a very strong correlation with time series of MODIS-based SCF over the TP, correlation coefficient as high as 0.75. This clearly indicates the limitation of current satellite-based QPE being incapable of adequately resolving winter precipitation.

(4) To reduce the still relatively large and complex uncertainty over the TP, three data merging methods are examined to provide the best possible satellite precipitation data by optimally combing the five state-of-art products. The three merging methods – arithmetic mean, inverse-error-square weight, and one-outlier-removed arithmetic mean – show insignificant yet subtle differences. Bias and RMSE of the three merging methods show seasonal dependency, but the one-outlier-removed method is more robust and its result notably outperforms the five individual products at the four seasons except the winter. The correlation coefficient by the three merging methods is consistently higher than any of the five individual satellite estimates, indicating an effective and great improvement. However, because of the large difference among satellite products in winter, the result from the ensemble is not always better than the best one among the five satellite products.

(5) Finally, the spatial distribution of the ensemble data is present against the five individual satellite estimates, which indicate that the ensemble can provide a general improvement over the entire studied region both at the seasonal and at the annual time scales. Comparing the number of each satellite product being taken as the outlier demonstrates that PERSIANN, TRMM 3B42RT, and NRL contribute more uncertainty, while TRMM 3B42 and CMORPH contribute less uncertainty. In warm seasons and at an annual time scale, combining CMORPH with TRMM 3B42 cannot provide overall better results than those from the one-outlier-removed method, but in winter it is still inferior to the result obtained from TRMM 3B42. TRMM 3B42 shows the best performance in wither over the TP. We recommend the result from the one-outlier-removed method as the best over the TP for the seasonal and annual time scales except for the winter, although these optimally merging multi-algorithm data appear a cost-effective way to provide better-quality satellite precipitation data presently. The recently launched Global Precipitation Measurement Mission, with dual-frequency precipitation radar and multi-frequency passive microwave channels, holds promising potential in this complex and high-altitude TP region, and the data from the GPM can further evaluate and verify the results in this article.

Funding

This work was supported by grants from Chinese Ministry of Science and Technology [2012BAC22B04]; China Meteorological Administration [GYHY201406001]; and National Natural Science Foundation of China [51379056, 41101375].

References

Adler, R. F., C. Kidd, G. Petty, M. Morissey, and H. M. Goodman. 2001. "Intercomparison of Global Precipitation Products: The Third Precipitation Intercomparison Project (PIP-3)." *Bulletin of the American Meteorological Society* 82: 1377–1396. doi:10.1175/1520-0477(2001)082<1377:IOGPPT>2.3.CO;2.

Adler, R. F., J. J. Wang, G. Gu, and G. J. Huffman. 2009. "A Ten-Year Tropical Rainfall Climatology Based on a Composite of TRMM Products." *Journal of the Meteorological Society of Japan* 87A: 281–293. doi:10.2151/jmsj.87A.281.

Behrangi, A., K.-L. Hsu, B. Imam, S. Sorooshian, G. J. Huffman, and R. J. Kuligowski. 2009. "PERSIANN-MSA: A Precipitation Estimation Method from Satellite-Based Multispectral Analysis." *Journal of Hydrometeorology* 10: 1414–1429. doi:10.1175/2009JHM1139.1.

Chen, S., P. E. Kirstetter, Y. Hong, J. J. Gourley, Y. D. Tian, Y. C. Qi, Q. Cao, J. Zhang, K. Howard, J. J. Hu, and X. W. Xue. 2013. "Evaluation of Spatial Errors of Precipitation Rates and Types from TRMM Space-borne Radar over the Southern CONUS." *Journal of Hydrometeorology* 14: 1884–1896. doi:10.1175/JHM-D-13-027.1.

Daly, C., R. P. Neilsen, and D. L. Phillips. 1994. "A Statistical Topographic Model for Mapping Climatological Precipitation over Mountainous Terrain." *Journal of Applied Meteorology* 33: 140–158. doi:10.1175/1520-0450(1994)033<0140:ASTMFM>2.0.CO;2.

Ebert, E. E., J. E. Janowiak, and C. Kidd. 2007. "Comparison of Near-Real-Time Precipitation Estimates from Satellite Observations and Numerical Models." *Bulletin of the American Meteorological Society* 88: 47–64. doi:10.1175/BAMS-88-1-47.

Hong, Y., K. L. Hsu, S. Sorooshian, and X. Gao. 2004. "Precipitation Estimation from Remotely Sensed Imagery Using an Artificial Neural Network Cloud Classification System." *Journal of Applied Meteorology* 43: 1834–1853. doi:10.1175/JAM2173.1.

Hsu, K. L., X. Gao, S. Sorooshian, and H. V. Gupta. 1997. "Precipitation Estimation from Remotely Sensed Information Using Artificial Neural Networks." *Journal of Applied Meteorology* 36: 1176–1190. doi:10.1175/1520-0450(1997)036<1176:PEFRSI>2.0.CO;2.

Hsu, K. L., H. V. Gupta, X. Gao, and S. Sorooshian. 1999. "Estimation of Physical Variables from Multichannel Remotely Sensed Imagery Using a Neural Network: Application to Rainfall Estimation." *Water Resources Research* 35: 1605–1618. doi:10.1029/1999WR900032.

Huffman, G. J., D. T. Bolvin, E. J. Nelkin, D. B. Wolff, R. F. Adler, G. Gu, Y. Hong, K. P. Bowman, and E. F. Stocker. 2007. "The TRMM Multisatellite Precipitation Analysis (TMPA): Quasi-Global, Multiyear, Combined-Sensor Precipitation Estimates at Fine Scales." *Journal of Hydrometeorology* 8: 38–55. doi:10.1175/JHM560.1.

Jeong, D., and Y. O. Kim. 2009. "Combining Single-Value Streamflow Forecasts – A Review and Guidelines for Selecting Techniques." *Journal of Hydrology* 377: 284–299. doi:10.1016/j.jhydrol.2009.08.028.

Joyce, R. J., J. E. Janowiak, P. A. Arkin, and P. P. Xie. 2004. "CMORPH: A Method That Produces Global Precipitation Estimates from Passive Microwave and Infrared Data at High Spatial and Temporal Resolution." *Journal of Hydrometeorology* 5: 487–503. doi:10.1175/1525-7541(2004)005<0487:CAMTPG>2.0.CO;2.

Li, S. J. 2011. "Forecasting Skill of Ensemble Mean: Theoretical Study and the Applications in the T213 and TIGGE EPSs." [In Chinese]. PHD degree, Department of Atmospheric Sciences, Nanjing University.

Luo, H. B., and M. Yanai. 1984. "The Large-Scale Circulation and Heat Sources over the Tibetan Plateau and Surrounding Areas during the Early Summer of 1979. Part II: Heat and Moisture Budgets." *Monthly Weather Review* 112: 966–989. doi:10.1175/1520-0493(1984)112<0966:TLSCAH>2.0.CO;2.

McLeod, A. I., D. J. Noakes, K. W. Hipel, and R. M. Thompstone. 1987. "Combining Hydrologic Forecasts." *Journal of Water Resources Planning and Management* 113: 29–41. doi:10.1061/(ASCE)0733-9496(1987)113:1(29).

Sanders, F. 1963. "On Subjective Probability Forecasting." *Journal of Applied Meteorology* 2: 191–201. doi:10.1175/1520-0450(1963)002<0191:OSPF>2.0.CO;2.

Shen, Y., M. N. Feng, H. Z. Zhang, and X. Gao. 2010. "Interpolation Methods of China Daily Precipitation Data." [In Chinese]. *Journal of Applied Meteorological Science* 21 279–286.

Shen, Y., A. Y. Xiong, Y. Wang, and P. P. Xie. 2010. "Performance of High-Resolution Satellite Precipitation Products over China." *Journal of Geophysical Research* 115: D02114. doi:10.1029/2009JD012097.

Smith, T. M., P. A. Arkin, J. J. Bates, and G. J. Huffman. 2006. "Estimating Bias of Satellite-Based Precipitation Estimates." *Journal of Hydrometeorology* 7: 841–856. doi:10.1175/JHM524.1.

Sorooshian, S., K. L. Hsu, X. Gao, H. Gupta, B. Imam, and D. Brainthwaite. 2000. "Evaluation of PERSIANN System Satellite-Based Estimates of Tropical Rainfall." *Bulletin of the American Meteorological Society* 81: 2035–2046. doi:10.1175/1520-0477(2000)081<2035:EOPSSE>2.3.CO;2.

Tian, Y., C. D. Peters-Lidard, B. J. Choudhury, and M. Garcia. 2007. "Multitemporal Analysis of TRMM-Based Satellite Precipitation Products for Land Data Assimilation Applications." *Journal of Hydrometeorology* 8: 1165–1183. doi:10.1175/2007JHM859.1.

Tian, Y. D., and C. D. Peters-Lidard. 2010. "A Global Map of Uncertainties in Satellite-Based Precipitation Measurements." *Geophysical Research Letters* 37: L24407. doi:10.1029/2010GL046008.

Tian, Y. D., C. D. Peters-Lidard, J. B. Eylander, R. J. Joyce, G. J. Huffman, R. F. Adler, K. Hsu, F. J. Turk, M. Garcia, and J. Zeng. 2009. "Component Analysis of Errors in Satellite-Based Precipitation Estimates." *Journal of Geophysical Research* 114: D24101. doi:10.1029/2009JD011949.

Turk, F. J., E. E. Ebert, B. J. Sohn, H. J. Oh, V. Levizzani, E. A. Smith, and R. Ferraro. 2003. "Validation of an Operational Global Precipitation Analysis at Short Time Scales." Proceedings of 12th Conference on Satellite Meteorology and Oceanography, American Meteorological Society, Long Beach, CA.

Winter, C. L., and D. Nychka. 2010. "Forecasting Skill of Model Averages." *Stochastic Environmental Research and Risk Assessment* 24: 633–638. doi:10.1007/s00477-009-0350-y.

Xie, P. P., M. Chen, S. Yang, A. Yatagai, T. Hayasaka, Y. Fukushima, and C. Liu. 2007. "A Gauge-Based Analysis of Daily Precipitation over East Asia." *Journal of Hydrometeorology* 8: 607–626. doi:10.1175/JHM583.1.

Yong, B., Y. Hong, L.-L. Ren, J. J. Gourley, G. J. Huffman, X. Chen, W. Wang, and S. I. Khan. 2012. "Assessment of Evolving TRMM-Based Multisatellite Real-Time Precipitation Estimation Methods and Their Impacts on Hydrologic Prediction in a High Latitude Basin." *Journal of Geophysical Research* 117 (D9): 1–21. doi:10.1029/2011JD017069.

Yoo, J. H., and I.-S. Kang 2005. "Theoretical Examination of a Multi-Model Composite for Seasonal Prediction." *Geophysical Research Letters* 32. doi:10.1029/2005GL023513.